catalysts

MDPI

Article

Upgrading V_2O_5-WO_3/TiO_2 deNO*x* Catalyst with TiO_2-SiO_2 Support Prepared from Ti-Bearing Blast Furnace Slag

Tuyetsuong Tran [1,2], Jian Yu [1,*], Lina Gan [1,2], Feng Guo [1], Dinhtuan Phan [1] and Guangwen Xu [1,*]

[1] State Key Laboratory of Multi-phase Complex Systems, Institute of Process Engineering, Chinese Academy of Sciences, Beijing 100190, China; ttsuong87@gmail.com (T.T.); lngan@ipe.ac.cn (L.G.); guofeng@ipe.ac.cn (F.G.); phantuan23bhht@gmail.com (D.P.)

[2] University of Chinese Academy of Sciences, Beijing 100049, China

* Correspondence: yujian@ipe.ac.cn (J.Y.); gwxu@ipe.ac.cn (G.X.); Tel.: +86-10-82544886 (J.Y.); +86-10-82629912 (G.X.)

Academic Editor: Keith Hohn

Received: 26 January 2016; Accepted: 29 March 2016; Published: 12 April 2016

Abstract: The study is devoted to developing a rather high-efficiency NH_3-SCR (selective catalytic reduction) catalyst for NO_x removal using TiO_2-SiO_2 support made from blast furnace slag. Through adjusting hydrolytic pH value of $TiOSO_4$ solution obtained from acidolysis of slag with 70 wt. % H_2SO_4, a series of TiO_2-SiO_2 mixed oxides was prepared to have different mass ratios of TiO_2 to SiO_2. The supports are further impregnated with V_2O_5 and WO_3 to make the SCR catalysts for NO_x removal. Characterizing the catalysts show that silica and unavoidable impurities in support prepared from slag were responsible for maintaining their mesoporous structure and the enhancements in the acidity and reducible form of active species on the catalyst surface, which thus rendered the catalysts to have higher NO_x reduction capability than catalyst using commercial TiO_2. Furthermore, the low-cost catalyst prepared from slag-based TiO_2 support possesses good stability, and strong resistance to SO_2 and H_2O poisoning, which are beneficial to practical deNO$_x$ applications.

Keywords: blast furnace slag; V_2O_5-WO_3/TiO_2-SiO_2; NH_3-SCR catalyst; deNO$_x$; flue gas

1. Introduction

Nitrogen oxides (NO_x) are the key pollutant for overall improvement of ambient air quality and multi-objective environmental management. In Asian countries such as China, the NO_x emission is predicted to increase further as a result from its economic development that causes fast growth of coal consumption [1–4]. Various technologies have been developed to control emissions of NO_x (deNO$_x$), mainly including the Selective Non-Catalytic Reduction by NH_3 (NH_3-SNCR), Selective Catalytic Reduction by NH_3 (NH_3-SCR) and oxidation absorption with liquid. Among them, NH_3-SCR is the most common technology for deep removal of NO_x from various kinds of flue gas. In this process, the NO_x in flue gas selectively reacts with gaseous ammonia over the catalyst to produce nitrogen and water without generating any secondary pollutants [5–7]. Currently, the global demand for SCR systems is increasing rapidly and China has the biggest market. The NH_3-SCR catalyst costs 40% of the entire investment and most widespread commercial SCR catalyst is based on V_2O_5/TiO_2 formulations, such as V_2O_5-WO_3/TiO_2 and V_2O_5-MoO_3/TiO_2 [7,8]. Technical development continues to seek "better" deNO$_x$ catalysts that possess high SCR performance, good resistance to SO_2 poisoning and low preparation cost [9–12]. A major way is to upgrade the porous TiO_2 support by incorporating with other metal oxides. Commercial titania fail to provide high surface area; however, to be used as a support for deNOx catalyst, titania should be characterized by high surface area and high onset temperature to rutilation. Thus, numerous metal oxides doped with TiO_2 have been studied

as mechanical promoters including Al_2O_3, SiO_2, Fe_2O_3, and CeO_2 for the improvement of $deNO_x$ catalytic activity [12–15]. Among various mixed oxides, TiO_2-SiO_2 has drawn special attention owing to its highly active in the SCR reaction and simultaneously, less active in the SO_2 oxidation reaction. A commercial V_2O_5-WO_3/TiO_2 usually has 0–10 wt. % silica introduced in catalyst molding [10,12]. Many reports in the literature [5,16–18] have reported that TiO_2-SiO_2 support can improve catalytic activity and SO_2 durability. Such superior low-temperature SCR activity was mainly attributed to the presence of polymeric vanadate species and high redox properties besides high surface area. The SO_2 oxidation activity was found to be significantly suppressed with increasing SiO_2 content in the support, which leads to a remarkable improvement of the sulfur tolerance of the catalyst and thus is favorable for industrial applications of SCR process. Raising the SiO_2 content beyond 10 wt. % decreased the realized NO conversion, due to the active-component transfer and NH_3 adsorption on strong acid sites [17–19].

Southwestern China is rich in magnetite bearing vanadium and titanium; its blast furnace slag (BFS) from iron-steel making process contain 20–22 wt. % TiO_2 [20]. This titanium-bearing BFS is quite different from ilmenite, which contains 40–50 wt. % TiO_2. The latter are currently used to produce TiO_2 support for SCR $deNO_x$ catalyst through sulfate method [21], where the ilmenite ore is dissolved in concentrated sulfuric acid solution to prepare a titanium sulfate solution ($TiOSO_4$). This solution is further purified and hydrolyzed to produce pure TiO_2 [21,22]. In China, only 25% of Ti-bearing BFS is used to make dam concrete or road-paving material. The accumulated Ti-slag has exceeded 70 million tons, and it still increases by a rate of three million tons per year in China [20,23]. This not only wastes its containing Ti resource but also causes serious environmental pollution [23]. The slag contains both TiO_2 and SiO_2, and it can potentially be converted into the TiO_2-SiO_2 support for $deNO_x$ catalyst. The use of TiO_2 made from slag as a support for NH_3-SCR catalyst is important in terms of lowering the catalyst cost and exploiting a new way to fully utilize the Ti-BFS.

The feasibility of making NH_3-SCR catalyst using Ti-bearing BFS based on sulfate method has been reported in our previous work [11]. The obtained catalyst showed even higher $deNO_x$ activity than that based on commercial TiO_2. This work continues to upgrade such a V_2O_5-WO_3/TiO_2 catalyst by using TiO_2-SiO_2 supports made from Ti-bearing BFS under varied hydrolytic conditions. The TiO_2-SiO_2 supports with different TiO_2/SiO_2 ratios are prepared to clarify how the $deNO_x$ activity of catalyst varies with the composition, structure and acidity of the prepared support. However, besides containing certain SiO_2, all samples made with slag had some unavoidable impurities such as Al_2O_3 and Fe_2O_3. The purifications of these impurities have been performed according to [24–26], but the process was too complicated and increased the preparation cost. As mentioned above, the incorporation of Al_2O_3 and Fe_2O_3 into TiO_2 as mechanical promoters helped to improve the SCR activity. An earlier study [13] also reported that the co-introduction of SiO_2 and Al_2O_3 into TiO_2 increased the resistance to SO_2 and H_2O poisoning in SCR of NO by NH_3. Thus, aim at minimizing the preparation cost, the obtained support from different hydrolytic conditions will be used directly without any other purification steps.

2. Results and Discussion

2.1. Composition Varying with Hydrolytic pH Value

The control of pH value is very important for hydrolysis of the $TiOSO_4$ solution obtained from acidolysis of BFS because the precipitation of SiO_2 is incomplete at pH values below 2.8 [27,28]. To achieve and maintain the pH value during hydrolysis, aqueous ammonia ($NH_3.xH_2O$ 25%) was slowly added into the formed $TiOSO_4$ solution. Four parallel of syntheses were formed and named as BFS-TiO_2 N with N (pH = 1, 2, 3), denoting the pH value, and further NA for the case without pH adjustment. During leaching, TiO_2, SiO_2, Al_2O_3, and MgO become soluble, whereas CaO remains as $CaSO_4$ residue [29]. The composition of precipitated products, as shown in Table 1, obviously varied with hydrolytic pH value, indicating the dependence on isoelectric points (IEPs) of different components in the solution.

Table 1. Yield and main chemical composition of BFS-TiO_2 supports obtained under different hydrolytic pH values (mass %).

Sample	Composition of Calcined Sample								Yield	
	TiO_2	SiO_2	MgO	CaO	Al_2O_3	Fe_2O_3	SO_4^{2-}	Others	TiO_2 Recovery	Total Product
Typical slag	20–23	22–25	7–8	27–28	14–15	-	-	-	-	-
Spent slag	20.9	23.2	10.3	27.0	13.8	1.4	1.7	1.7	-	-
NA (not adjusted)	92.2	6.8	-	-	0.1	0.1	0.5	0.3	73.6	78.1
pH =1	87.7	9.2	-	-	0.6	1.4	0.4	0.7	75.0	82.7
pH =2	79.9	14.5	-	-	2.5	2.5	0.3	1.3	76.8	88.9
pH =3	81.6	11.1	-	-	2.9	3.0	0.3	1.1	78.6	92.7
Residue	1.2	20.9	0.2	24.1	0.3		52.9	0.4	-	-

For SiO_2, its electrical mobility is zero at pH between 2 and 3, and the rate of aggregation for silica sol particles gets its minimum in this range of pH. Thus, the content of SiO_2 in precipitate increased to 14.5 wt. % when pH value was raised to 2 and then slightly decreased with higher pH values. Meanwhile, iron oxides and alumina sol started to precipitate from the solution and their amounts slowly increased with raising pH of the $TiOSO_4$ solution for hydrolysis. This trend is consistent with the result in Seggiani *et al.* [27] who reported that with the rise in pH value the positive charge of anions decreased until a certain point was reached to cause negative adsorption of anions, at pH values of 6–7 for Al_2O_3 and 8.4–8.6 for Fe_2O_3 [27,28,30]. Besides, the positively-charged species cannot effectively be adsorbed onto the positively-charged anatase TiO_2 surface (IEP = 3.5). Therefore, only little iron oxides and alumina gel were deposited on TiO_2. Furthermore, the recovery ratio of TiO_2 also varied with pH value for the four prepared samples. At pH of 3, the realized highest yield of total precipitate and TiO_2 recovery ratio were 92.7% and 78.6%, respectively. The total product yield was found to increase with raising pH value of hydrolysis solution since more impurities were co-precipitated at higher pH values.

2.2. Structure of Prepared Supports

Figure 1a compares the shapes of adsorption isotherms for a commercial TiO_2 sample and several synthetic BFS-TiO_2 samples. According to the IUPAC (International Union of Pure and Applied Chemistry) classification, the isotherms of all BFS-TiO_2 are almost type IV to show obvious mesoporous structure in the samples [31]. Meanwhile, the TiO_2 support belongs to the type H1, implying a uniform cylindrical pore geometry in the material. In all the synthetic BFS-TiO_2 samples, the shape and location of their hysteresis loops vary with the hydrolytic conditions, and the physical properties of the produced TiO_2 are strongly subject to the incorporated Si. The isotherm for the BFS-TiO_2 NA sample is actually a mixture of the types H2 and H3 hysteresis loops, but that for the BFS-TiO_2 samples at pH = 1–3 belongs to the type H2. Thus, the mesopores in all BFS-TiO_2 supports are irregular in size and shape [31]. From Figure 1b we can see that the pore size distribution (PSDs) moves towards smaller sizes when increasing the SiO_2 content to cause collapse of inter-aggregated pores, as represented by the hysteresis loop at high P/P_0 [32]. The contribution of SiO_2 to the formation of pores in BFS-TiO_2 was also proven by the increased surface area and decreased mean pore sizes with the rise of SiO_2 content. Interestingly, the PSDs change from a bimodal structure for the commercial TiO_2 and BFS-TiO_2 NA to a unimodal mesopore structure for the BFS-TiO_2 samples made at pH = 1–3 which contain silica and oxide dopants like Al_2O_3 and Fe_2O_3 in high amounts. This indicates that both silica and impurities in the supports help to maintain their high mesopore fraction, resulting the greater surface area shown in Table 2 [33]. Generally, a large pore volume is due to a high fraction of mesopores with high and non-uniform surface area (H2 and H3 hysteresis loops), which improves the catalytic activity by obtaining better dispersion of vanadium species on support and facilitating the spread of reactant molecules (NO) to active sites existing in the meso-structure framework [7,34]. All of this suggests that

both silica and impurities in the slag-based deNO$_x$ catalyst facilitate the catalytic NH$_3$-SCR reactions, especially for the support made at pH 1 that has the largest mesopore volume.

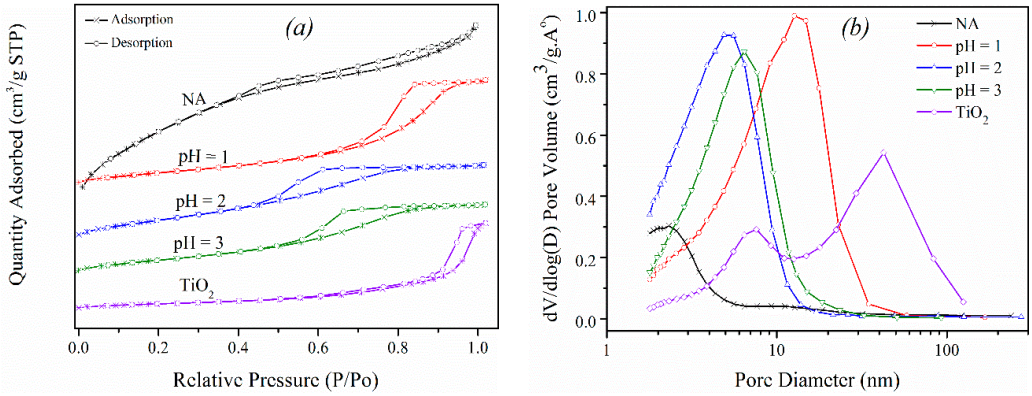

Figure 1. Characterization of BFS-TiO$_2$ and TiO$_2$ supports: (**a**) isotherms of N$_2$ adsorption and desorption; and (**b**) pore size distribution.

Table 2. Structural parameters of supports and loading amount of active components for their catalysts.

Sample	Support				Catalyst	
	BET ($m^2 \cdot g^{-1}$)	Pore Size (nm)	Pore Volume ($cm^3 \cdot g^{-1}$)	Crystalline Size (nm) [a]	V_2O_5 Load (%)	WO_3 Load (%)
TiO$_2$	119.32	15.99	0.477	21.22	1.9	4.8
NA	172.24	3.13	0.135	14.89	2.2	4.9
pH = 1	282.28	8.62	0.609	11.90	2.0	5.1
pH = 2	427.61	4.41	0.471	7.43	2.0	4.9
pH = 3	298.02	5.62	0.419	8.47	1.9	5.1

[a] TiO$_2$ crystalline size was calculated from X-ray diffraction (XRD) data.

The microstructures of synthetic BFS-TiO$_2$ samples have been studied using SEM (Scanning Electron Microscopy) and TEM (Transmission Electron Microscopy) analysis, presented in Figure 2. It could be observed from SEM images Figure 2(a,d) that the BFS-TiO$_2$ supports possess a rough porous surface accompanied with many mesopores (TEM images Figure 2b,e) to imply high surface area and high adsorptive capacity [35]. The micrographs also revealed that the secondary particles, as observed in Figure 2(a,d), comprise agglomerated irregular primary particles, of which the size was dependent on hydrolytic pH value, as observed in Figure 2(b,e) [35]. Meanwhile, SEM image showed that the BFS-TiO$_2$ NA support had a broad size distribution and two types of aggregates, namely elongated shape and mainly spherical shape with loosely agglomerated. The micrographs of BFS-TiO$_2$ samples with pH adjustment were very similar and represented by sample prepared at pH 1; their SEM showed the asymmetric plate-like morphology with larger, more consolidated agglomerates, thus exposing new textural properties (see Figure 1) in comparison to sample without pH adjustment in hydrolysis. The severe agglomeration observed in samples having pH adjustment is probably because the strong acidity of the initial hydrolysis solution caused slow hydrolyzation; the enhancement in the hydrolytic pH value might have helped to increase in reaction rate that led to increase the number of particles and, consequently, the number of collisions leading to agglomeration [21,36,37].

Further identification of the configuration of morphology was achieved by TEM and HRTEM images. TEM analysis revealed that the synthetic BFS-TiO$_2$ supports had obviously spherical primary particles without any coating on the surface [21]. A high resolution transmission electron microscopic (HRTEM) study was performed to clarify the distribution of crystalline titania within the BFS-TiO$_2$ samples. All the observed lattice fringes of BFS-TiO$_2$ nanoparticles show a d-spacing of 0.360 nm, which can be well assigned to the (101) lattice fringes of anatase TiO$_2$ (d = 0.352 nm, JCPDS No. 21-1272), confirming the presence of anatase TiO$_2$ in all the BFS-TiO$_2$ supports [38].

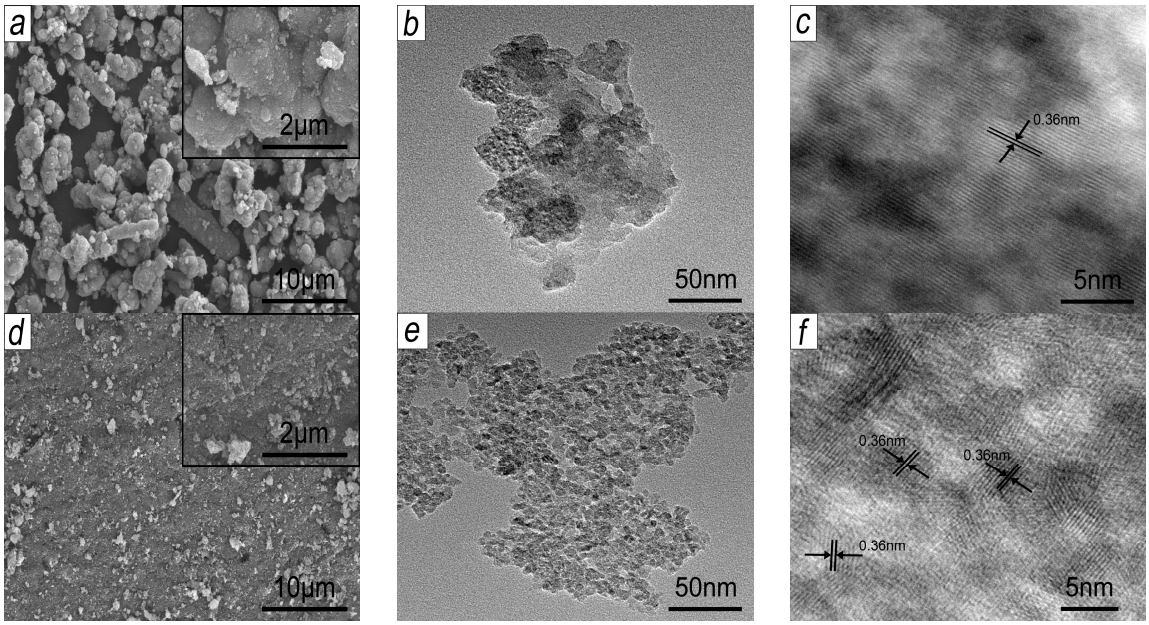

Figure 2. SEM, TEM and HRTEM micrographs of BFS-TiO_2 samples made at different pH values of hydrolysis: (**a**–**c**) NA; and (**d**–**f**) pH 1.

In order to further understand the structure of BFS-TiO_2 from hydrolysis under different pH values, FT-IR (Fourier Transform Infrared Spectroscopy) spectra were taken for all tested supports (Figure 3). For this characterization, each sample was dried at 200 °C for 2 h to remove free water. Usually, the IR broad band at 400–850 cm^{-1} is accepted to be the stretching vibration of Ti–O bonds in Ti–O–Ti [39]. Meanwhile, the broad band at 3200–3600 cm^{-1} is attributed to the stretching vibration of –OH of adsorbed water as well as surface hydroxyl, and that at 1635 cm^{-1} is assigned to the bending vibration of –OH. For all synthetic BFS-TiO_2 samples, the new absorption bands at 1100 cm^{-1} and 960 cm^{-1} are induced by the stretching vibration of Si–O–Si and Ti–O–Si bonds, respectively. The IR results suggest that BFS-TiO_2 is a composite of TiO_2 and SiO_2, and that Ti–O–Si bond is formed between TiO_2 and SiO_2 particles [40].

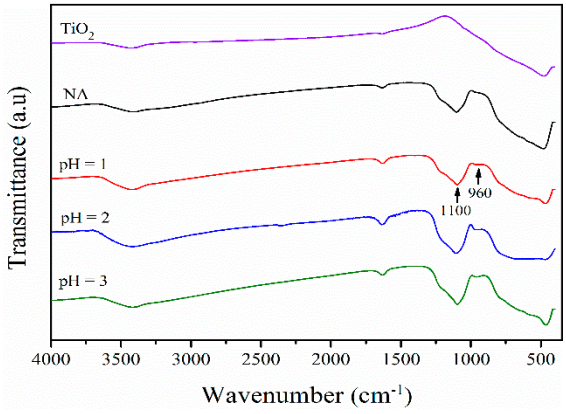

Figure 3. FT-IR spectra of different synthetic BFS-TiO_2 samples and commercial TiO_2.

The crystallographic phase shown in Figure 4 can be identified as anatase TiO_2, which is in accordance with TEM results. For all BFS-TiO_2 samples, no pronounced change was observed in the XRD pattern, except for a lower intensity than that for pure TiO_2. The lattice aberrances turn bigger for all BFS-TiO_2 containing higher silica content, which is consistent with the literatures [39,40].

According to the Scherrer's formula, the sizes of the anatase crystallites was between 14.9–7.4 nm, as listed in Table 2. The suppression in crystalline size together with the formation of Ti–O–Si bond proved by FT-IR spectra indicated that SiO_2 is uniformly incorporated into titania lattice and no peaks corresponding to SiO_2 were observed, suggesting the formation of amorphous SiO_2 [40]. Furthermore, the presence of SiO_2 in BFS-TiO_2 does not allow structural changes except for a slight shift towards higher 2θ values due to shrinkage of the pores, thereby stabilizing the meso-structures [41]. Neither impurities, Al_2O_3 nor Fe_2O_3, are detected, probably because of their weakness compared to the strong scattering from anatase, suggesting that impurities well dispersed over the surface of titania or existed as an amorphous phase [13,14]. The difference in crystallinity is not proportional to reflect the enabled NO_x conversion because the support also has different acidities and acid sites. The acidity of support is associated with NH_3 adsorption on catalyst, which should increase with raising acidity [12,17].

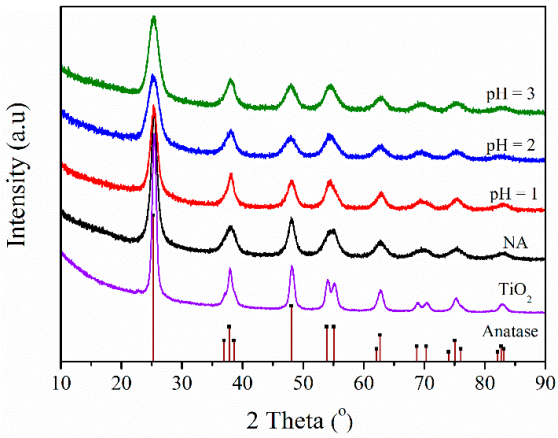

Figure 4. XRD patterns of different synthetic BFS-TiO_2 samples and commercial TiO_2.

The temperature programmed desorption (TPD) of NH_3 is a well-known method for determination of acidic properties of solid heterogeneous catalysts. In the NH_3–TPD curves, peaks are generally distributed into two regions: below and above 400 °C, referred to as low-temperature (LT) and high-temperature (HT) regions, respectively. The peaks in the HT region can be attributed to the desorption of NH_3 from strong acid sites, and the peak in the LT region is assigned as the desorption of NH_3 from some relatively weak acid sites [42]. NH_3-TPD profiles of synthetic BFS-TiO_2 and TiO_2 supports, presented in Figure 5, showed broadly distributed acid sites in the LT region. In general, their TPD curves are similar in shape but clearly different in magnitude. The signal of all BFS-TiO_2 samples greatly increased as compared to pure TiO_2, which meant the density of acid sites was enhanced with the incorporation of SiO_2. The formation of Ti–O–Si band was believed to develop more acid sites [42,43]. This result implies that the presence of SiO_2 in BFS-TiO_2 samples brought more active NH_3 adsorbed species, which is reported to be significantly beneficial to SCR reaction [9,13,17]. The amount of NH_3 desorbed on the samples has increased with the increase of SiO_2 content [9], indicating that more acidic sites occurred in the catalyst having higher SiO_2 content and the weak acid sites are predominant [39].

H_2-Temperature programmed reduction (H_2-TPR) measurements were conducted to characterize the reduction performances and the interactions of dispersed active species with support [12]. As shown in Figure 6, H_2-TPR profiles of different catalysts from supports with varied TiO_2/SiO_2 ratios are characterized by two broad peaks with their T_{max} around 431–483 °C and 742–848 °C, indicating the reductions of V_2O_5 and WO_3, respectively. The different reduction properties of V_2O_5 and WO_3 on BFS-TiO_2 supports was observed, illustrating their different interactions with support [44]. It can be seen in Figure 6 that the catalysts from BFS-TiO_2 showed larger peak areas than that from commercial TiO_2. As we all know, a catalyst possessing a larger reduction peak means the more reducible form of active species on the catalyst surface, which has a positive effect on NO catalytic

reduction with NH_3 [45]. These results demonstrated that the incorporation of SiO_2 to BFS-TiO_2 support is beneficial to disperse VO_x and WO_x species on the surface than pure TiO_2 support did [12]. Additionally, T_{max} of reduction peak for mainly active VO_x species also reflects the difficulty of its valence change during deNO_x reaction, which is directly related to the deNO_x activity of a catalyst. The reduction peaks of VO_x species shift to lower temperature region, thus the reduction reaction takes place more easily [12,44]. One can see that the VO_x reduction peaks firstly shifted to low temperature with raising the amount of SiO_2 in support, suggesting that the reducibility of some surface vanadium oxide species increases with increasing silica [17,46]. Surprisingly, the T_{max} value of VO_x species in the catalyst having the highest SiO_2 content (BFS-TiO_2 pH 2) is significantly higher than that of both other BFS-TiO_2 samples and commercial TiO_2, suggesting that the modification of titania by high content of SiO_2 seems to decrease the reducibility of surface vanadium oxide species and that a strong interaction exists between the surface vanadium oxide and surface silica species, resulting in the difficult reduction. Such observation has also been reported by Gao *et al.* [46], which verifies the TiO_2/SiO_2 ratio in 1 wt.% V_2O_5/TiO_2-SiO_2 to study reducibility properties of catalyst and type of the surface VO_x species on the support. T_{max} of VO_x reduction was found to be the lowest for the catalyst with the support at pH = 1, suggesting stronger redox properties for this sample.

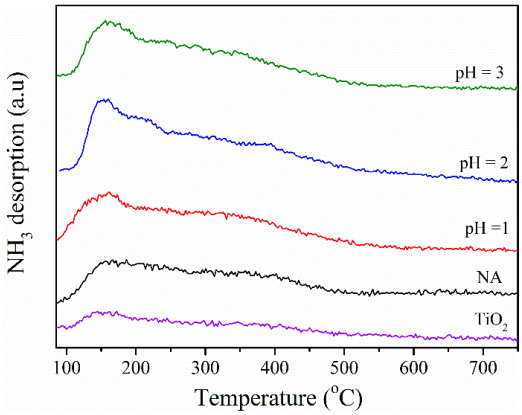

Figure 5. NH_3-TPD patterns of BFS-TiO_2 samples made at different pH values of hydrolysis and commercial TiO_2.

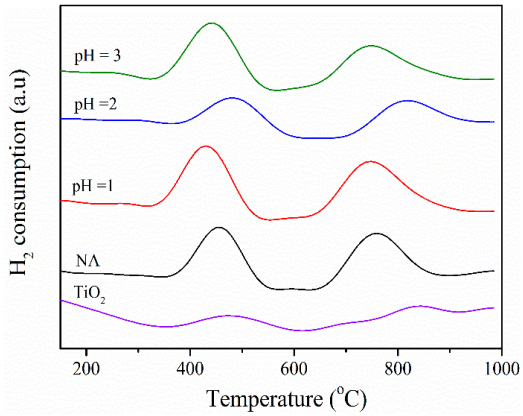

Figure 6. H_2-TPR profiles of catalysts on commercial TiO_2 and BFS-TiO_2 made at different pH values of hydrolysis (2 wt. % V_2O_5, 5 wt. % WO_3).

2.3. Catalytic Performance of Catalysts

The activity test in the reduction of NO by NH_3 was carried out over catalysts prepared by impregnating 2 wt. % V_2O_5 and 5 wt. % WO_3 on the prepared BFS-TiO_2 and commercial TiO_2 as

support. Evaluation of catalysts was conducted at 150–500 °C in simulated flue gas and the results are compared in Figure 7. The catalytic activity increased with raising temperature from 150 °C to 400 °C and then sharply decreased at rather higher temperatures, which was caused by the parallel oxidation of NH_3 by O_2, resulting a decrease in the amount of NH_3 participating in the SCR of NO [44]. In 200–400 °C, the best deNO_x efficiency was shown for V_2O_5-WO_3/BFS-TiO_2 (pH = 1) with 9.2 wt. % SiO_2 in its support, whereas the lowest activity was for the catalyst on BFS-TiO_2 (pH = 2) with the highest SiO_2 content of 14.5 wt. %. The catalyst made with the commercial TiO_2 without any SiO_2 exhibited higher catalytic activity than that with BFS-TiO_2 (pH = 2) did. Meanwhile, the catalysts on the supports made with pH = 3 and NA (no pH adjustment) had a similar catalytic activity at all temperatures tested. These obvious differences in catalytic activity among the catalysts should be subject to different compositions, pore structures and acidic properties of used supports.

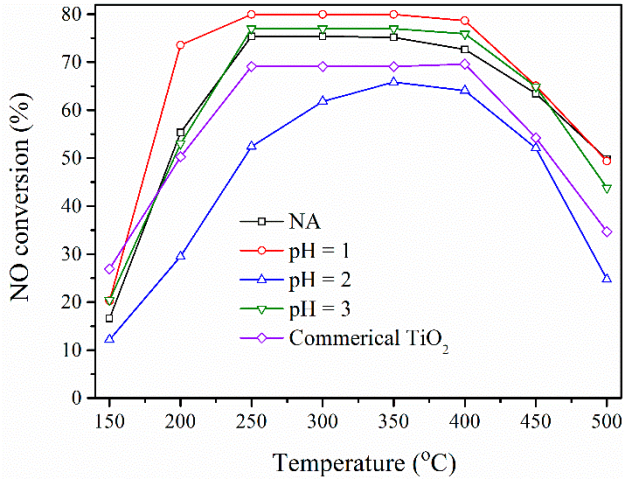

Figure 7. NO conversion *versus* temperature for catalysts with 2 wt. % V_2O_5 and 5 wt. % WO_3 on BFS-TiO_2 and commercial TiO_2 supports.

The high surface area, surface acidity coupled with the more reducible form of VO_x and WO_x species on the surface of catalysts prepared from BFS-TiO_2 supports allowed an enhancement of the catalytic efficiency in the SCR of NO by NH_3 as compare to catalyst prepared from pure TiO_2 [12,45]. The deNO_x activity of slag-based catalysts increased with the increase of SiO_2 content up to 9.2 wt. % (BFS-TiO_2 pH 1) and then decreased. It was obvious that the total acidic strength of BFS-TiO_2 pH 2 having the highest SiO_2 content was greater than that of the other catalysts, but the NO conversion over this catalyst was the lowest. An earlier study of V_2O_5/TiO_2–SiO_2 by Kobayashi *et al.* [17] reported that this behavior was attributed to the difference in the NH_3 adsorption capacity. It is considered that NH_3 is not utilized effectively for the transformation of NO to N_2 since NH_3 is too strongly adsorbed on the large number of acidic sites in a large concentration of SiO_2, which is reversely disadvantageous for SCR reaction. Moreover, a strong interaction exists between the surface vanadium oxide and surface silica species caused the difficult reducibility of VO_x species, resulting its low catalytic activity [46]. Table 3 listed the distribution of VO_x reduction peak from H_2-TPR results and the reaction rate constant (k_{mass}) for comparison of catalytic activity irrespective of the small loading deviations occurred during impregnation process. The results revealed that the reaction rate constant of the prepared catalyst complies with their H_2-TPR profile. The best redox performance and the highest reaction rate constant shown for the support made at pH = 1 had the highest mesopore volume. Pinnavaia *et al.* [34] reported that sample having high mesopore volume can facilitate the diffusion of reactant molecules (NO) or reaction intermediates to active sites on the mesoporous support. These results verify that the amount of SiO_2 content catalyst support does have great effect on the redox properties of surface VO_x species, surface acidity and textural properties, and, consequently, affects the NO catalytic reduction with NH_3 [12,17,46].

Table 3. Position of VO_x peak maxima (T_{max}) obtained from H_2-TPR analysis and the mass rate constant (k_{mass}) at 300 °C of NO-NH_3 reaction.

Sample	TiO_2	NA	pH = 1	pH = 2	pH = 3
T_{max} of VOx (°C)	476	455	431	483	441
k_{mass} ($cm^3/g.s$)	116.8	131.6	150.0	93.1	140.0

In practical use, the SCR reaction atmosphere usually contains some fraction of H_2O and SO_2. Therefore, the effect of 10 vol. % H_2O and 600 ppm of SO_2 on the SCR reaction over the catalyst on BFS-TiO_2 at pH = 1 and commercial TiO_2 supports was investigated. The experiments were performed at 300 °C with an NH_3/NO ratio of 0.8 and GSHV of 24,000 h^{-1}. Figure 8 revealed that the presence of steam and SO_2 in the feed inhibited significantly the NH_3-SCR reaction over these catalysts, especially V_2O_5-WO_3/TiO_2 catalyst. For catalyst prepared from BFS-TiO_2 support, the presence of steam lowered NO conversion by about 5%, but still retained a stable NO conversion to N_2 in an 8-h test, and stopping the feed of H_2O soon restored its catalytic activity. However, with the presence of both SO_2 and steam, the NO conversion was stabilized at a value about 10% lower than that for the gas without SO_2 and steam; furthermore stopping SO_2 and steam (~24 h), the NO conversion again restored quickly to a high value. The same trends were also observed over catalyst made with commercial TiO_2, a significant reduction from 66% to 45% in NO conversion was observed when gas feed contained both SO_2 and steam. Nonetheless, its catalytic activity recovered gradually and did not recover to the original level after stopping the feed of SO_2 and steam. Literature studies found that the most significant reason for maintaining a high activity of catalyst on TiO_2-SiO_2 support in the presence of SO_2 and steam is due to the special network structure of the Ti-Si that can suppress the sulfate formation the surface of the Ti-Si binary oxide support [12,13,17,19]. These results suggest that the catalyst made with the slag-based TiO_2 support (by pH = 1) can enhance the catalytic activity and possesses good stability, strong resistance to SO_2 and H_2O poisoning, which are beneficial to practical deNO_x applications as compared to catalyst prepared from commercial TiO_2 support.

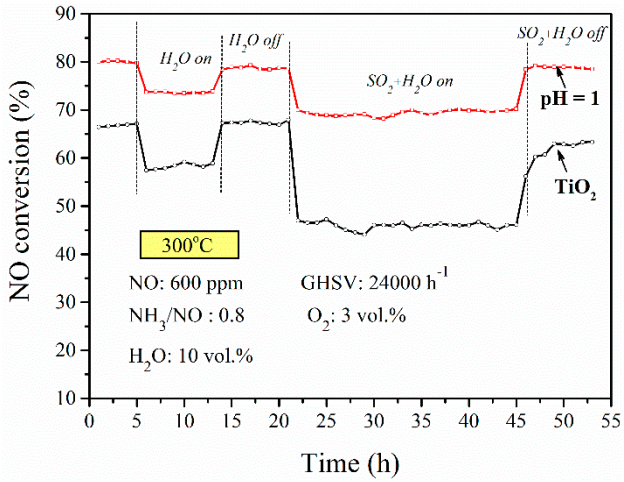

Figure 8. Resistance to poisoning of SO_2 and steam for the catalyst prepared with commercial TiO_2 support and BFS-TiO_2 support made at pH = 1 of hydrolysis (2 wt. % V_2O_5, 5 wt. % WO_3).

3. Experimental Section

3.1. Slag Treatment and Catalyst Preparation

The raw Ti-bearing blast furnace slag (BFS) was provided by Panzihua Iron & Steel Group Co., Ltd. in China. Prior to use, the slag was dried and crushed into particle sizes below 0.2 mm. Then, the XRF analysis was applied to determine slag composition, as shown in Table 1. Figure 9 shows the XRD

pattern of the slag. A broad diffraction peak around 30° was identified to be CaO-SiO_2-Al_2O_3-TiO_2 glass structure [47], and there was no anatase TiO_2 diffraction peak. Thus, the BFS needs to be treated for getting anatase TiO_2 used as the support of SCR catalyst [17,19].

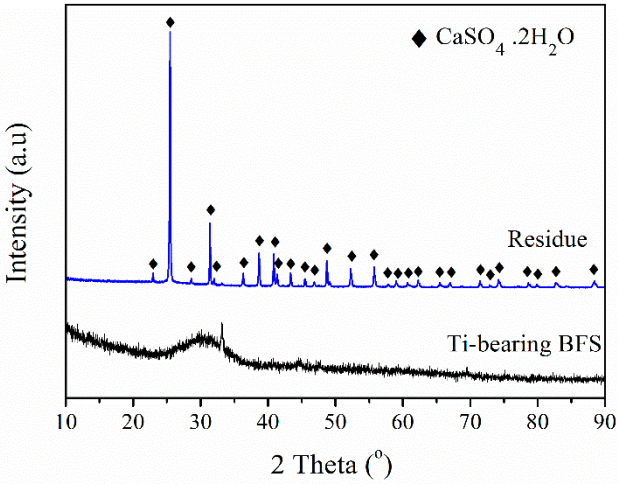

Figure 9. XRD patterns of treated blast furnace slag (BFS) and leaching residue.

Studies on ilmenite leaching with sulfuric acid clarified that the maximal dissolution rate of ilmenite occurs at 70–76 wt. % H_2SO_4 at 88–100 °C [21,22]. The leaching was thus conducted using 70 wt. % sulfuric acid at 90 °C and lasted for 3 h. The mass ratio of H_2SO_4 over BFS was maintained at 1.5. Figure 9 also shows that the *residue of leaching* mainly consists of anhydrite ($CaSO_4 \cdot 2H_2O$, JCPDS 01-072-0503) and 1.2 wt. % TiO_2 (XRF analysis). This confirms that nearly all TiO_2 was dissolved by sulfuric acid [29]. The black $TiOSO_4$ solution formed by this acidolysis was further hydrolyzed to make precipitates through adjusting the hydrolytic pH to a value of 1, 2 or 3 using 25% aqueous ammonia. For hydrolysis, the $TiOSO_4$ solution was first hydrolyzed at 80 °C for 5 h and then reacted at 110 °C for 5 h to form a H_2TiO_3 slurry. By filtration and washing further, the obtained filter cake was finally dried at 110 °C and calcined at 600 °C for 4 h to transform H_2TiO_3 into anatase TiO_2. The total product yield and recovery percent of TiO_2 are calculated (Equations (1) and (2)):

$$\text{Total product yield } (\%) = \frac{\text{The calcined gel}}{TiO_2 \text{ in the slag}} \times 100, \quad (1)$$

$$TiO_2 \text{ recovery } (\%) = \frac{TiO_2 \text{ in calcined gel}}{TiO_2 \text{ in the slag}} \times 100 \quad (2)$$

In order to carry out catalytic activity comparison between slag-based catalysts and the most widespread commercial V_2O_5-WO_3/TiO_2-based SCR catalyst at the same amount of active species, the anatase TiO_2 employed as a deNO_x catalyst support was prepared by calcination of metatitanic acid (H_2TiO_3 99%, Chengdu XiYa Chemical Technology Co., Chengdu, China) at 600 °C for 4 h.

In turn, the deNO_x catalyst V_2O_5-WO_3/BFS-TiO_2 and V_2O_5-WO_3/TiO_2 was prepared according to the successive impregnation method using ammonium paratungstate ($[NH_4]_6W_7O_{24} \cdot 6H_2O$), Sinopharm, Shanghai, China) and ammonium metavanadate (NH_4VO_3, Sinopharm, Shanghai, China) as precursors for W and V, respectively. Firstly, the supports were added into the $[NH_4]_6W_7O_{24} \cdot 6H_2O$ solution and the slurry was dryness under continuous stirring at 60 °C until the solution became a paste, then drying at 110 °C for 10 h took place. After that, NH_4VO_3 was dissolved in oxalic acid (10 wt. %) to form the blue complex vanadyl oxalate $VO(C_2O_4)_2$. The above obtained powder was introduced into this solution and the slurry was brought to dryness under continuous stirring at 60 °C until the solution became a paste. Finally, the paste was dried at 110 °C for 10 h and calcined at 600 °C for 4 h. All the catalysts were made to have the same composition of metal oxides, 2 wt. % V_2O_5,

5 wt. % WO_3 and balanced TiO_2. Besides, all the used materials and solvents for catalyst preparation and experiments were commercially bought.

3.2. Characterization and Evaluation

XRD measurement was carried out in 2θ angles of 10–90° on a D/Max-RB diffractometer (Rigaku Corp., Tokyo, Japan) with Cu Kα radiation. Nitrogen *adsorption/desorption* isotherms were recorded on an ASAP 2020 (Micromeritics Instrument Corp., Norcross, GA, USA) at 77 K. All the products were degassed in vacuum at 150 °C for 6 h prior to BET measurements. The Brunauer–Emmett–Teller (BET) equation was used to calculate the specific surface area (S_{BET}). Pore size distributions were calculated from the adsorption branch using the Barret–Joyner–Halenda (BJH) model, while the nitrogen adsorption volume at the relative pressure (P/P_o) of 0.994 was used to determine the pore volume and average pore size. XRF analysis in the Axios X-ray fluorescence (XRF) spectrometer (PANalytical X'pert, Almelo, The Netherlands) was performed to determine the sample composition. Scanning electron microscopy (SEM) images were recorded at 10 kV on JSM-7001F electron microscopy (JEOL Ltd., Tokyo, Japan), samples were coated with Au prior to analysis and imaged directly. Transmission electron microscopy (TEM) observation was carried out on a JEM-2100 of JEOL transmission electron microscope (JEOL, Tokyo, Japan) at an accelerating voltage of 200 kV, TEM samples were mounted on a copper-supported carbon polymer grid by placing a few droplets of a suspension of the ground sample in ethanol on the grid, followed by drying at ambient conditions. Transmission FT-IR spectra were recorded from Bruker Tensor 27 instrument (Bruker, Rheinstetten, Germany) in the 400–4000 cm^{-1} resolution, 1 mg dry powder was dispersed into 100 mg an IR transmissive material (KBr) and pressed to obtain transparent disks.

NH_3-TPD and H_2-TPR measurements were carried out on the ChemBET Pulsar TPR/TPD equipment from Quantachrome Instruments (FL, USA). Firstly, 0.1 g of sample was loaded into a quartz U-tube and heated from room temperature to 300 °C at 10 °C.min^{-1} and then maintained there for 150 min in a Helium atmosphere. In turn, the sample was cooled to 90 °C and was further followed by heating to 700 °C at 5 °C· min^{-1} for NH_3-TPD or to 1000 °C at 5 °C· min^{-1} for H_2-TPR in a gas flow of 30 mL· min^{-1}. The consumed NH_3 or H_2 in the process of temperature rise was continuously monitored on-line using a mass spectrometry (Proline Mass Spectrometer, Ametek, PA, USA).

Catalytic activity measurement for SCR of NO by NH_3 was conducted in a quartz fixed bed reactor of 15 mm in internal diameter under atmospheric pressure. The tested catalyst was powder with particle sizes below 0.2 mm, and the simulated flue gas consisted of 0.06 vol. % NO, 0.048 vol. % NH_3, 3 vol. % O_2, 10 vol. % H_2O, 0.06 vol. % SO_2 and balanced N_2. The total flow rate through the reactor was 400 mL· min^{-1} (STP) to give a Gas Hourly Space Velocity (GHSV) of 24,000 h^{-1} for activity test in two case studies, absence and presence of SO_2 and steam in the reaction stream. Taking this high space velocity was for evidently comparing the activities of different catalysts. The molar concentrations of gases entering and exiting the reactor were continually monitored using a using a PG-300 portable gas analyzer from Horiba Ltd. (Kyoto, Japan). The reaction usually reached a steady state after about 1 h at a given temperature, and the realized NO conversion [7] was calculated according to the measured inlet and outlet NO concentrations (Equation (3)):

$$X_{NO}\ (\%) = \frac{NO_{in} - NO_{out}}{NO_{in}} \times 100 \quad (3)$$

The reaction rate constant (k_{mass}) for the maximal deNO_x efficiency was calculated by assuming a pseudo-first order SCR reaction with respect to NO and zero order to NH_3 [7] (Equation (4)):

$$k = -\frac{V^*}{W} \times \ln(1 - X_{NO}), \quad (4)$$

where V* is the total flow rate under reaction conditions, W the loaded amount of active component and X_{NO} the NO conversion.

4. Conclusions

NO_x removal catalysts with low cost and good SCR performance were prepared using BFS-TiO_2 support made from blast furnace slag (BFS). In hydrolysis of $TiOSO_4$ solution obtained from acidolysis of slag, the hydrolytic pH value was varied to control the precipitation of metal components and thus the properties of the obtained BFS-TiO_2 support such as composition, structure and acidic properties. All synthetic BFS-TiO_2, which contained certain SiO_2 and unavoidable impurities Al_2O_3 and Fe_2O_3, had mesoporous structure with high BET surface area of about 172–427 m^2/g. The incorporated SiO_2 in BFS-TiO_2 samples was responsible for the enhancement in the amount of NH_3 adsorbed and the reducible species formed on the catalyst surface, which enabled them to have good activity for catalyzing NO-NH_3 reaction in comparison to the commercial TiO_2 support. However, deNO_x efficiency over V_2O_5-WO_3 supported on BFS-TiO_2 pH 2 (having the highest SiO_2 content) is significantly lower than that of both other BFS-TiO_2 samples and commercial TiO_2. This suggested that the modification of titania by high content of SiO_2 caused difficulty in reducibility of VO_x in its catalyst due to the strong interaction between the surface VO_x and surface SiO_2 species; and strongly NH_3 adsorbed on its catalyst surface is subjected to the suppression of NH_3 participating in the SCR of NO to N_2. The best deNO_x efficiency, nearly 80% NO conversion at an NH_3/NO ratio of 0.8 in 200–400 °C for the catalyst prepared from BFS-TiO_2 pH 1, which also showed fairly good ability of resistance to the SO_2 and steam poisoning. All of these show in fact that V_2O_5 and WO_3 loaded on BFS-TiO_2 pH 1 having 9.2 wt. % of SiO_2 is suitable as SCR catalyst for practical deNO_x application due to high activity in SCR, good stability, strong resistance to SO_2 and steam poisoning, and, especially, low preparation catalyst cost.

Acknowledgments: The authors are grateful to the financial supports of International Science and Technology Cooperation Program of China (2013DFA51530), Strategic Priority Research Program of Chinese Academy of Sciences (XDA07030300), and Japan Society for the Promotion of Science (JSPS) for the postdoctoral fellowship grant (P15758).

Author Contributions: The experimental work was conceived and designed by T.T., J.Y. and G.X. T.T. performed the experiments; T.T, J.Y. and G.X. analyzed the data; L.G. and F.G. contributed reagents/materials/analysis tools; and T.T, J.Y., D.P. and G.X. drafted the paper. The manuscript was amended through the comments of all authors. All authors have given approval for the final version of the manuscript.

Conflicts of Interest: The authors declare no conflict of interest.

References

1. Wang, S.X.; Zhao, B.; Cai, S.Y.; Klimont, Z.; Nielsen, C.P.; Morikawa, T.; Woo, J.H.; Kim, Y.; Fu, X.; Xu, J.Y.; *et al.* Emission trends and mitigation options for air pollutants in East Asia. *Atmos. Chem. Phys.* **2014**, *14*, 6571–6603. [CrossRef]
2. Felix, J.D.; Elliott, E.M.; Shaw, S.L. Nitrogen isotopic composition of coal-fired power plant NO_x: Influence of emission controls and implications for global emission inventories. *Environ. Sci. Technol.* **2012**, *46*, 3528–3535. [CrossRef] [PubMed]
3. Tian, H.; Liu, K.; Hao, J.; Wang, Y.; Gao, J.; Qiu, P.; Zhu, C. Nitrogen oxides emissions from thermal power plants in China: Current status and future predictions. *Environ. Sci. Technol.* **2013**, *47*, 11350–11357. [CrossRef] [PubMed]
4. Zhao, B.; Wang, S.X.; Liu, H.; Xu, J.Y.; Fu, K.; Klimont, Z.; Hao, J.M.; He, K.B.; Cofala, J.; Amann, M. Nox emissions in China: Historical trends and future perspectives. *Atmos. Chem. Phys.* **2013**, *13*, 9869–9897. [CrossRef]
5. Shan, W.; Song, H. Catalysts for the selective catalytic reduction of NO_x with NH_3 at low temperature. *Catal. Sci. Technol.* **2015**, *5*, 4280–4288. [CrossRef]
6. Wang, Y.; Zhang, H.; Wang, J. NO_x sensor reading correction in diesel engine selective catalytic reduction system applications. *IEEE/ASME Trans. Mech.* **2016**, *21*, 460–471. [CrossRef]

7. Marberger, A.; Elsener, M.; Ferri, D.; Kröcher, O. VO_x surface coverage optimization of V_2O_5/WO_3-TiO_2 SCR catalysts by variation of the V loading and by aging. *Catalysts* **2015**, *5*, 1704–1720. [CrossRef]
8. China SCR Denitration Catalyst Industry Report, 2013–2016. PRNewswire, 8 January 2014.
9. Peng, Y.; Liu, C.; Zhang, X.; Li, J. The effect of SiO_2 on a novel CeO_2–WO_3/TiO_2 catalyst for the selective catalytic reduction of NO with NH_3. *Appl. Catal. B* **2013**, *140–141*, 276–282. [CrossRef]
10. Casanova, M.; Schermanz, K.; Llorca, J.; Trovarelli, A. Improved high temperature stability of NH_3-SCR catalysts based on rare earth vanadates supported on TiO_2-WO_3-SiO_2. *Catal. Today* **2012**, *184*, 227–236. [CrossRef]
11. Yang, J.; Lei, S.; Yu, J.; Xu, G.W. Low-cost V−W−Ti SCR catalyst from Titanium-bearing blast furnace slag. *J. Environ. Chem. Eng.* **2014**, *2*, 1007–1010. [CrossRef]
12. Pan, Y.; Zhao, W.; Zhong, Q.; Cai, W.; Li, H. Promotional effect of Si-doped V_2O_5/TiO_2 for selective catalytic reduction of NO_x by NH_3. *J. Environ. Sci.* **2013**, *25*, 1703–1711. [CrossRef]
13. Zhao, W.; Tang, Y.; Wan, Y.; Li, L.; Yao, S.; Li, X.; Gu, J.; Li, Y.; Shi, J. Promotion effects of SiO_2 or/and Al_2O_3 doped CeO_2/TiO_2 catalysts for selective catalytic reduction of NO by NH_3. *J. Hazard. Mater.* **2014**, *278*, 350–359. [CrossRef] [PubMed]
14. Yang, S.; Wang, C.; Ma, L.; Peng, Y.; Qu, Z.; Yan, N.; Chen, J.; Chang, H.; Li, J. Substitution of WO_3 in V_2O_5/WO_3-TiO_2 by Fe_2O_3 for selective catalytic reduction of NO with NH_3. *Catal. Sci. Technol.* **2013**, *3*, 161–168. [CrossRef]
15. Matralis, H.K.; Ciardelli, M.; Ruwet, M.; Grange, P. Vanadia catalysts supported on mixed TiO_2-Al_2O_3 supports: Effect of composition on the structure and acidity. *J. Catal.* **1995**, *157*, 368–379. [CrossRef]
16. Granger, P.; Parvulescu, V.I. Catalytic NO_x abatement systems for mobile sources: From three-way to lean burn after-treatment technologies. *Chem. Rev.* **2011**, *111*, 3155–3207. [CrossRef] [PubMed]
17. Kobayashi, M.; Kuma, R.; Masaki, S.; Sugishima, N. TiO_2-SiO_2 and V_2O_5/TiO_2-SiO_2 catalyst: Physico-chemical characteristics and catalytic behavior in selective catalytic reduction of NO by NH_3. *Appl. Catal. B: Environ.* **2005**, *60*, 173–179. [CrossRef]
18. Kobayashi, M.; Hagi, M. V_2O_5-WO_3/TiO_2-SiO_2-SO_4^{2-} catalysts: Influence of active components and supports on activities in the selective catalytic reduction of NO by NH_3 and in the oxidation of SO_2. *Appl. Catal. B: Environ.* **2006**, *63*, 104–113. [CrossRef]
19. Liu, C.; Chen, L.; Li, J.; Ma, L.; Arandiyan, H.; Du, Y.; Xu, J.; Hao, J. Enhancement of activity and sulfur resistance of CeO_2 supported on TiO_2–SiO_2 for the selective catalytic reduction of NO by NH_3. *Environ. Sci. Technol.* **2012**, *46*, 6182–6189. [CrossRef] [PubMed]
20. Zhang, L.; Zhang, L.N.; Wang, M.Y.; Li, G.Q.; Sui, Z.T. Recovery of titanium compounds from molten ti-bearing blast furnace slag under the dynamic oxidation condition. *Miner. Eng.* **2007**, *20*, 684–693. [CrossRef]
21. Li, Z.; Wang, Z.; Li, G. Preparation of Nano-Titanium Dioxide from ilmenite using sulfuric acid-decomposition by liquid phase method. *Powder Technol.* **2016**, *287*, 256–263. [CrossRef]
22. Liang, B.; Li, C.; Zhang, C.; Zhang, Y. Leaching kinetics of panzhihua ilmenite in sulfuric acid. *Hydrometallurgy* **2005**, *76*, 173–179. [CrossRef]
23. Chen, D.-S.; Zhao, L.-S.; Qi, T.; Hu, G.-P.; Zhao, H.-X.; Li, J.; Wang, L.-n. Desilication from titanium–vanadium slag by alkaline leaching. *Trans. Nonferrous Met. Soc. China* **2013**, *23*, 3076–3082. [CrossRef]
24. Xiong, X.; Wang, Z.; Wu, F.; Li, X.; Guo, H. Preparation of TiO_2 from ilmenite using sulfuric acid decomposition of the titania residue combined with separation of Fe^{3+} with edta during hydrolysis. *Adv. Powder Technol.* **2013**, *24*, 60–67. [CrossRef]
25. Liu, S.-S.; Guo, Y.-F.; Qiu, G.-Z.; Jiang, T.; Chen, F. Preparation of Ti-rich material from titanium slag by activation roasting followed by acid leaching. *Trans. Nonferrous Met. Soc. China* **2013**, *23*, 1174–1178. [CrossRef]
26. Lasheen, T.A. Sulfate digestion process for high purity TiO_2 from titania slag. *Front. Chem. Eng. China* **2009**, *3*, 155–160. [CrossRef]
27. Seggiani, M.; Vitolo, S. Recovery of silica gel from blast furnace slag. *Resour. Conserv. Recycl.* **2003**, *40*, 71–80. [CrossRef]
28. Rouseková, I.; Bajza, A.; Živica, V. Silica fume-basic blast furnace slag systems activated by an alkali silica fume activator. *Cem. Concr. Res.* **1997**, *27*, 1825–1828. [CrossRef]

29. Valighazvini, F.; Rashchi, F.; Nekouei, R.K. Recovery of titanium from blast furnace slag. *Ind. Eng. Chem. Res.* **2013**, *52*, 1723–1730. [CrossRef]
30. Sverjensky, D.A. Zero-point-of-charge prediction from crystal chemistry and solvation theory. *Geochim. Cosmochim. Acta* **1994**, *58*, 3123–3129. [CrossRef]
31. Sing, K.; Everett, D.; Haul, R.; Moscou, L.; Pierotti, R.; Rouquerol, J.; Siemieniewska, T. Reporting physisorption data for gas/solid systems with special reference to the determination of surface area and porosity. *Pure Appl. Chem.* **1985**, *57*, 603–619. [CrossRef]
32. Yu, J.; Yu, J.C.; Leung, M.K.P.; Ho, W.; Cheng, B.; Zhao, X.; Zhao, J. Effects of acidic and basic hydrolysis catalysts on the photocatalytic activity and microstructures of bimodal mesoporous titania. *J. Catal.* **2003**, *217*, 69–78. [CrossRef]
33. Kim, J.; Song, K.C.; Foncillas, S.; Pratsinis, S.E. Dopants for synthesis of stable bimodally porous titania. *J. Eur. Ceram. Soc.* **2001**, *21*, 2863–2872. [CrossRef]
34. Pinnavaia, T.J.; Pauly, T.R.; Kim, S.S. Mesoporous molecular sieve catalysis: Relationships between reactivity and long range structural order/disorder. In *Supported Catalysts and Their Applications*; Sherrington, D.C., Kybett, A.P., Eds.; The Royal Society of Chemistry: London, UK, 2001; pp. 19–26.
35. Ngamta, S.; Boonprakob, N.; Wetchakun, N.; Ounnunkad, K.; Phanichphant, S.; Inceesungvorn, B. A facile synthesis of nanocrystalline anatase TiO_2 from $TiOSO_4$ aqueous solution. *Mater. Lett.* **2013**, *105*, 76–79. [CrossRef]
36. Park, H.K.; Park, K.Y.; Jung, K.Y. Alumina-precursor nanoparticles prepared by partial hydrolysis of $AlCl_3$ vapor in tubular flow reactor: Effect of hydrolysis conditions on particle size distribution. *Ind. Eng. Chem. Res.* **2014**, *53*, 10372–10379. [CrossRef]
37. French, R.A.; Jacobson, A.R.; Kim, B.; Isley, S.L.; Penn, R.L.; Baveye, P.C. Influence of ionic strength, pH, and cation valence on aggregation kinetics of titanium dioxide nanoparticles. *Environ. Sci. Technol.* **2009**, *43*, 1354–1359. [CrossRef] [PubMed]
38. Park, I.-S.; Jang, S.-R.; Hong, J.S.; Vittal, R.; Kim, K.-J. Preparation of composite anatase TiO_2 nanostructure by precipitation from hydrolyzed $TiCl_4$ solution using anodic alumina membrane. *Chem. Mater.* **2003**, *15*, 4633–4636. [CrossRef]
39. Ren, C.; Qiu, W.; Chen, Y. Physicochemical properties and photocatalytic activity of the TiO_2/SiO_2 prepared by precipitation method. *Sep. Purif. Technol.* **2013**, *107*, 264–272. [CrossRef]
40. Dong, R.-L.; Na, C.; Zhang, H.-P.; Chen, Z.-D.; Jin, C.-C. TiO_2/SiO_2 mesoporous microspheres with intelligently controlled texture. *Mater. Des.* **2016**, *89*, 830–838. [CrossRef]
41. Saha, J.; Mitra, A.; Dandapat, A.; De, G. TiO_2 nanoparticles doped SiO_2 films with ordered mesopore channels: A catalytic nanoreactor. *Dalton Trans.* **2014**, *43*, 5221–5229. [CrossRef] [PubMed]
42. Yan, X.-M.; Mei, P.; Xiong, L.; Gao, L.; Yang, Q.; Gong, L. Mesoporous titania-silica-polyoxometalate nanocomposite materials for catalytic oxidation desulfurization of fuel oil. *Catal. Sci. Technol.* **2013**, *3*, 1985–1992. [CrossRef]
43. Jin, R.; Wu, Z.; Liu, Y.; Jiang, B.; Wang, H. Photocatalytic reduction of NO with NH_3 using Si-doped TiO_2 prepared by hydrothermal method. *J. Hazard. Mater.* **2009**, *161*, 42–48. [CrossRef] [PubMed]
44. Wang, C.; Yang, S.; Chang, H.; Peng, Y.; Li, J. Dispersion of tungsten oxide on SCR performance of V_2O_5-WO_3/TiO_2: Acidity, surface species and catalytic activity. *Chem. Eng. J.* **2013**, *225*, 520–527. [CrossRef]
45. Youn, S.; Song, I.; Kim, D.H. Promotional effect on selective catalytic reduction of NO_x with NH_3 over overloaded W and Ce on V_2O_5/TiO_2 catalysts. *J. Nanomater.* **2015**, 1–7. [CrossRef]
46. Gao, X.; Bare, S.R.; Fierro, J.L.G.; Wachs, I.E. Structural characteristics and reactivity/reducibility properties of dispersed and bilayered $V_2O_5/TiO_2/SiO_2$ catalysts. *J. Phys. Chem. B* **1999**, *103*, 618–629. [CrossRef]
47. Ren, S.; Zhao, Q.; Yao, L.; Liu, Q. Precipitation behavior of perovskite and anosovite crystals from high ti-bearing blast furnace slag with small amount of B_2O_3. *Cryst. Eng. Comm.* **2016**, *18*, 1393–1402. [CrossRef]